Contact Resistance for "End-Contacted" Metal−Graphene and Metal−Nanotube Interfaces from Quantum Mechanics

Yuki Matsuda, Wei-Qiao Deng, and William A. Goddard III*

Materials and Process Simulation Center, California Institute of Technology, Pasadena, California 91125

Received: July 21, 2008; Revised Manuscript Received: June 29, 2010

In this paper, we predict the current−voltage ($I-V$) characteristics and contact resistance of "end-contacted" metal electrode−graphene and metal electrode−carbon nanotube (CNT) interfaces for five metals, Ti, Pd, Pt, Cu, and Au, based on the first-principles quantum mechanical (QM) density functional and matrix Green's function methods. We find that the contact resistance (normalized to surface C atoms) is 107 kΩ for Ti, 142 kΩ for Pd, 149 kΩ for Pt, 253 kΩ for Cu, and 187 kΩ for Au. This can be compared with the contact resistance (per C) for "side-contacted" metal−graphene or metal−CNT interfaces of 8.6 MΩ for Pd, 34.7 MΩ for Pt, 630 MΩ for Cu, etc. Those are in good agreement with available experimental results, 40.5 MΩ for Pt, for example. Thus, compared to the values for side-contacted interfaces from QM, we find a decrease in contact resistance by factors ranging from 6751 for Au and 2488 for Cu, to 233 for Pt and 60 Pd, to 8.8 for Ti. This suggests a strong advantage for developing technology to achieve "end-contacted" configurations.

1. Introduction

Carbon nanotubes (CNTs)[1] and graphenes (monolayer,[2,3] bilayer,[4,5] and nanoribbons[6,7]) are the most promising materials for applications in nanoelectronics due to their small size and superior electrical properties. In particular, metallic CNTs and graphenes are potential candidates for the on-chip interconnect materials in future integrated circuits[8−10] because they have potential advantages for achieving the highest possible density integration in combination with high current density,[11] ballistic conductance,[12−14] and high thermal conductivity.[15] Indeed, significant progress has been made in fabrication techniques for CNT interconnects on Si wafers. For example, CNT via (vertical) interconnects were successfully grown directly on Si wafers using Co,[16] Fe,[17] or Ni[18] catalysts. In addition, CNT horizontal interconnects have been integrated with silicon complementary metal-oxide-semiconductor (CMOS) transistors on the same chip through application of electric fields in ethanol, enabling above 1 GHz operation.[19] Single layer graphene has been demonstrated to exhibit high electron mobility (∼15 000 $cm^2/(V\ s)$) and thermal conductivity (3100−5300 Ω/mK).[2,20,21] Graphenes may have advantages over CNTs for developing strategies of selective growth on metals or semiconductors, for example, epitaxial growth on SiC(0001)[4,6,22] and Ru(0001).[23]

A critical property for such nanoelectronic devices is the contact resistance at the metal−CNT or metal−graphene interfaces. We previously reported contact resistances for the "side-contacted" metal electrode (Figure 1b) to CNT or graphene.[24] There we used ab initio quantum mechanical (QM) studies to show that Ti leads to the lowest contact resistance of 24.2 $k\Omega/nm^2$ followed by Pd (221 $k\Omega/nm^2$), Pt (881 $k\Omega/nm^2$), Cu (16.3 $M\Omega/nm^2$), and Au (32.6 $M\Omega/nm^2$) for the "side-contacted" metal electrode (Figure 1b) to CNT or graphene.[25] Although the Cu−graphene interface has a contact resistance 672 times higher for Ti, we found that incorporation of bifunctional groups (anchors) can reduce the Cu−graphene contact resistance by a factor of 275, making Cu better than Pd by 3.7 times.[25]

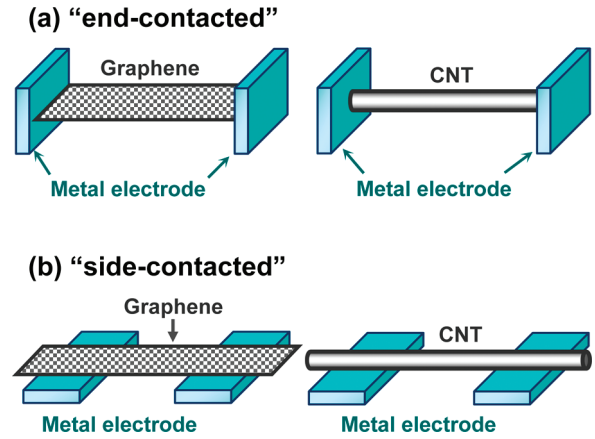

Figure 1. (a) Metal−graphene "end-contacted" interface. (b) "Side-contacted" interface.[24]

In this paper, we use QM to determine the electrical properties (e.g., contact resistance) for "end-contacted" (or vertical) metal−graphene and metal−CNT electrodes (Figure 1a). We find that this "end-contacted" metal electrode improves the contact resistance by up to a factor of 6751 while simultaneously increasing mechanical stabilities dramatically.

2. Methods

2.1. Modeling Details. To model the "end-contacted" metal−graphene or metal−CNT configurations shown in Figure 1a, we use the 2 × 4 graphene unit cell (16 carbon atoms) of the graphene sheet (fixed in the x direction at 0.846 nm), as shown in Figure 2. We placed the metal atoms at the arm-chair edge of graphene (four carbon atoms at the interface) one by one, followed by relaxing the geometry each time to determine the ideal metal−graphene interface. The six metal surface atoms that bond to four graphene carbon atoms at the interface (shown with red atoms in Figure 2) have a periodicity similar to the

* Author to whom correspondence should be addressed. Phone: (626) 395-2731. Fax: (626) 585-0918. E-mail: wag@wag.caltech.edu.

10.1021/jp806437y
Published on Web 09/23/2010

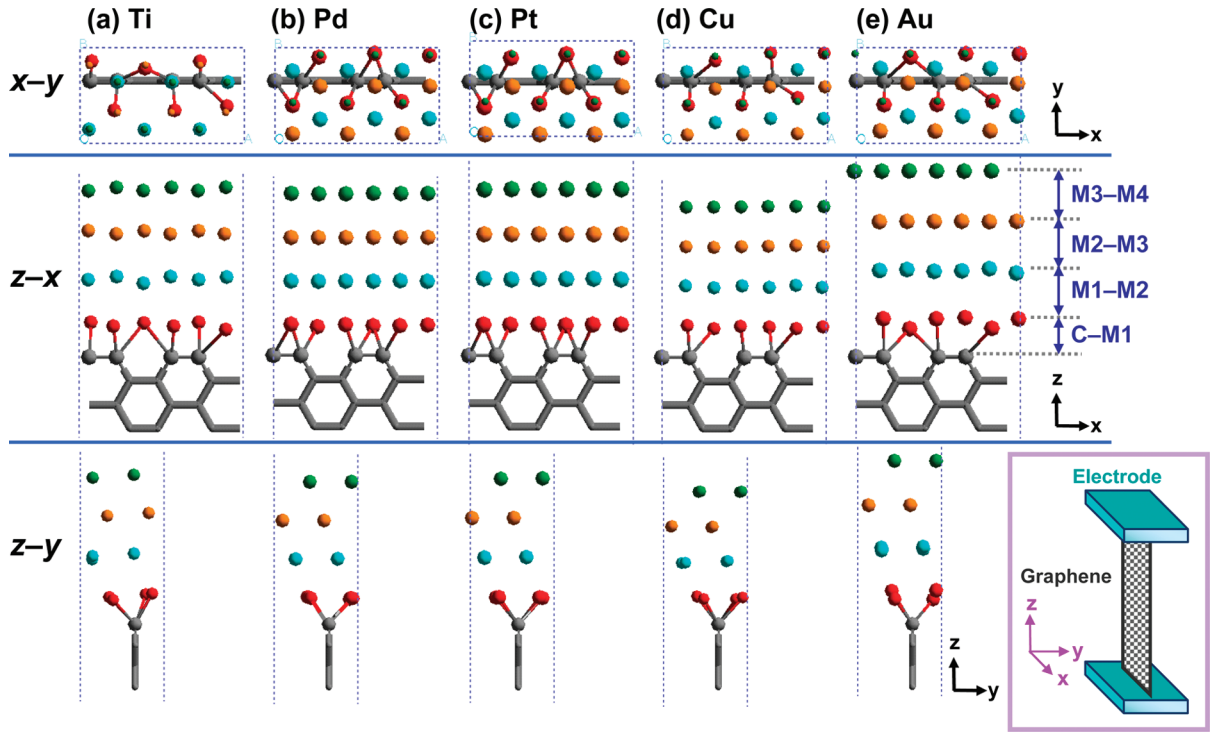

Figure 2. Optimized geometries for the graphene−metal interface (see Table 1 for quantitative values). The top section shows the top view ($x-y$ plane). The middle section shows the side view ($z-x$ plane). The bottom section shows the side view ($z-y$ plane). (a) Ti, (b) Pd, (c) Pt, (d) Cu, and (e) Au. The unit cell is 0.846 nm × 0.489 nm (periodic in $x-y$ directions) with 24 metal atoms (6 atoms × 4 layers) and 16 carbon atoms (4 atoms × 4 layers). The metal layers are built up atom by atom, leading to an hcp packing for Ti, while the others are found to have fcc packing. The layer−layer distances are given in Table 1 (C, graphene layer at the interface; M1, metal layer at the interface (first layer); M2, second metal layer; M3, third metal layer; M4, fourth metal layer).

TABLE 1: Structural Parameter Calculations for the Metal−Graphene Structures after Optimization, the Cohesive Energy (kcal/mol) of the Interface between Metal−Graphene and Layer−Layer Perpendicular Separations (Å)

	Ti	Pd	Pt	Cu	Au
C−M1 perpendicular separation[a] (Å)	1.65	1.54	1.59	1.55	1.79
M1−M2 perpendicular separation[a] (Å)	2.36	2.27	2.34	2.08	2.63
M2−M3 perpendicular separation[a] (Å)	2.39	2.24	2.30	2.06	2.53
M3−M4 perpendicular separation[a] (Å)	2.22	2.26	2.30	2.04	2.59
bulk value (experimental) 300 K[b] (Å)	2.34	2.25	2.26	2.08	2.36
metal−graphene cohesive energy[c] (kcal/mol)	77.4	55.9	54.4	45.2	29.6
metal−graphene cohesive energy of "side-contacted" structures[d] (kcal/mol)	6.0	0.28	0.21	0.14	0.12

[a] The Z-coordinates of the atoms are averaged. C, graphene layer at the interface; M1, metal layer at the interface (first layer); M2, second metal layer; M3, third metal layer; M4, fourth metal layer. C and M1−M4 are shown in Figure 2. [b] Reference 32. [c] Per surface C atom at the interface. [d] Per surface C atom. For comparison, see ref 24.

deposited metals on the sides of the graphene sheet in our previous work,[24] leading to a y periodicity of 0.489 nm. For each system, the metal atoms were added one by one and optimized for the contact to graphene. The additional three layers of metal (six atoms per layer per cell) were found to have ABC stacking (face-centered cubic (fcc)) for Pd, Pt, Cu, and Au and ABAB stacking (hexagonal close-packed (hcp)) for Ti for the bulk structures. For Ti, hcp packing was found to be more stable than fcc by 2.4 kcal/mol per unit cell.[24]

These models were used to study the local interfacial structures and contact resistance (R_{cont}) properties in this paper. The total resistance (R_T) is expressed as $R_T = R_{cont} + R_C +$ scattering, where R_C represents the resistance of CNT or graphene.[26] The scattering term can be ignored, since the distance is much smaller than the mean free path of an electron.

In our studies of side-contacted metal−carbon nanotube interfaces, we found that the metal−carbon bonds at the interface for the 0.95 nm diameter CNT (7,7) are reduced by 0.04A (1.9%) compared to metal−graphene while for the 1.0 nm diameter CNT (8,8) it is reduced by 0.08A (2.8%). Thus, the metal−graphene side-contacted interface is a good model for the metal−CNT side-contacted interface for CNT with diameters larger than 1.0 nm. For end-contacted interfaces, the curvature of the CNT would require much larger unit cells. However, from simple force field models, we considered that the covalent bonding of the armchair CNT to the metal would lead to a distribution of metal−carbon geometries similar to those for the graphene edge. Hence, we focus the QM calculations on the metal−graphene interface. Then, to predict the properties for the metal−CNT interface, we normalize on the basis of the number of carbons in the interface. We consider that this should be reliable for CNTs having diameters larger than 1.0 nm.

2.2. Computational Details. We used SEQQUEST,[27] a fully self-consistent Gaussian-based linear combination of atomic orbitals (LCAO) density functional theory (DFT) method with double-ζ plus polarization (DZP) basis sets.[28] All calculations

were based on the Perdew−Burke−Ernzerhof (PBE) flavor of generalized gradient approximation (GGA) with PBE pseudopotentials.[29] We use 2D periodic boundary conditions in the xy plane. On the basis of systematic energetic convergence studies, we selected the 4×4 k-point sampling in the Brillouin zone with a real space grid interval of 46×26 in the $x-y$ plane leading to a grid spacing of 0.35 bohr.

To determine the current−voltage ($I-V$) characteristics for each system, we first solved for the self-consistent wave functions using DFT quantum mechanics. The partial density of states (DOS) from these calculations are shown in various figures.

Then, we considered the layer of metal atoms on each side of the graphene to be part of the tunneling system and used the remaining three layers of atoms to determine the surface electrode Green function. Then, the transmission coefficient was obtained using matrix Green function theory based on the Hamiltonian matrix elements DFT (which we have used successfully to compute transport properties of molecular electronic devices).[30] The atomic projection of density of states is normalized on the basis of the nature of the transmission channels.[30] The $I-V$ characteristics are calculated by using the Landauer−Buttiker formula with known transmission coefficient.[30,31] The zero-bias transmission $T(E, V = 0)$ approximation was applied to the computation of the current I at a finite bias voltage (V), defined as the difference between the source and the drain voltage. We expect the finite-V transmission $T(E, V)$ to be close to $T(E)$ for low bias voltages of −0.1 to 0.1 V, the likely operating voltage range for devices studied in this paper. For voltages greater than 0.5 V, $I-V$ curves should be taken as qualitative.

After calculating the current as a function of bias voltage, we fitted the curves and used this fit to determine the contact conductance and contact resistance for the five deposited metals.

3. Results

3.1. Geometrical Properties. Figure 2 and Table 1 show the optimized geometries for the "end-contacted" metal−graphene interface of the optimum geometries. We see that metal−metal interlayer distances are generally within 2% of the bulk values[32] except for the top (vacuum) layer of Ti which is contracted by 5%, the top layer of Pt which is contracted by 3%, and the Au system for which all layers are increased ∼11%.

The interaction energy of each metal−graphene structure was calculated by comparing the equilibrium energy with the energy of each component after separating the electrode (all metal atoms) infinitely far from the graphene surface (snap bond energy) (Figure 3a). These quantities were normalized by the number (four) of surface C atoms at the interface.

We see that the bond energies range from 77.4 kcal/mol (Ti) to 29.6 kcal/mol (Au), decreasing as Ti > Pd ≈ Pt > Cu > Au. As expected, "end-contacted" electrodes lead to greatly increasing interaction energy over that of "side-contacted" electrodes (Figure 3b). The biggest improvement is for Cu with 323 times followed by Pt (259 times), Au (247 times), and Pd (199 times), with the smallest improvement for Ti with 12.9 times.

3.2. $I-V$ Characteristics. ***3.2.1. QM Calculations.*** The structures for the $I-V$ calculations (Figure 4a) were constructed from the optimized geometries (Figure 2) by reversing the electrodes and two surface carbon layers of the graphene. This leads to two contacts (source and drain) bridged by the channel (graphene). Since the surface layer of metal electrodes is strongly bonded to the graphene edge, this layer is included as part of the channel while the other three periodic layers of each

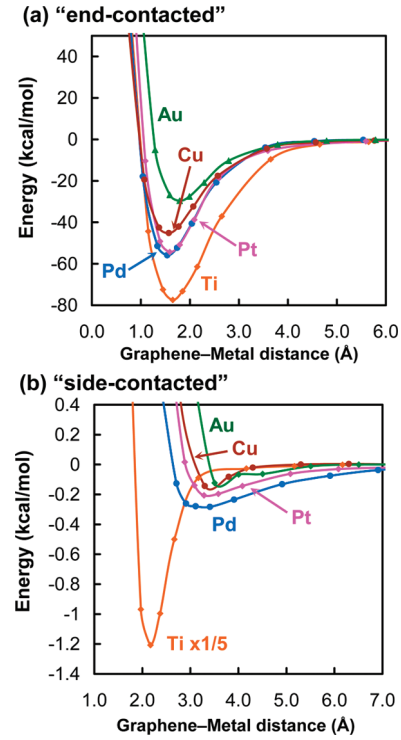

Figure 3. Interaction energy (per surface C atom) of (a) the metal−graphene "end-contacted" interface shown in Figure 1a and (b) the "side-contacted" interface shown in Figure 1b. The Ti is scaled by 1:5 (orange, Ti; blue, Pd; pink, Pt; brown, Cu; green, Au). The energies are given in Table 1.

electrode are considered to be the contact (used iteratively to form the surface Green function). Thus, the final system used in the $I-V$ calculations has xx atoms per unit cell.

We find that the DOS near the Fermi energy (Figure S1, Supporting Information) for the surface atoms has significant contributions only from the d orbitals of surface metals and the p orbitals of surface carbon atoms.

The projected density of states (PDOS) per unit cell of the p orbitals (PDOS(C_p)) of surface carbon atoms of graphene at the interface are shown in Figure 4b. These PDOS(C_p) differ substantially from each other with little systematic similarities in various peaks, reflecting the coupling with individual characteristics of the metal electrodes. Even so, the PDOS(C_p) are large and similar at the Fermi energy, ranging from 1.8 eV^{-1} (Ti) to 2.2 eV^{-1} (Au), indicating a good conduction channel. For the Ti, Pd, and Pt structures, the PDOS(C_p) of surface carbon atoms near the Fermi energy are mostly C pπ orbitals (py orbitals in Figure S1, Supporting Information), but for the Cu and Au structures, both pπ and pσ orbitals (py and pz orbitals, respectively, in Figure S1, Supporting Information) contribute equally.

The PDOS for the d orbitals of the surface (first-layer) metal atoms (PDOS(M_d)) are shown in Figure 4c. Here, we see the PDOS(M_d) at the Fermi energy ranging from 15 eV^{-1} (Ti) down to 1.5 eV^{-1} (Au) with a sequence of Ti > Pt > Pd > Cu > Au. For Au, the PDOS(C_p) is larger than the PDOS(M_d).

3.2.2. Tunneling Calculations. The transmission function, $T(E)$ (Figure 4d), near the Fermi energy mirrors the PDOS behavior except for the Cu system, which shows lower $T(E)$ than the Au system at the Fermi energy (−0.5 to +0.25 eV). The calculated $I-V$ curve (Figure 5a) and total resistance (Figure 5b) correlate directly with $T(E)$, which correlates with the cohesive coupling between the metal d orbitals and graphene p orbitals, as discussed above.

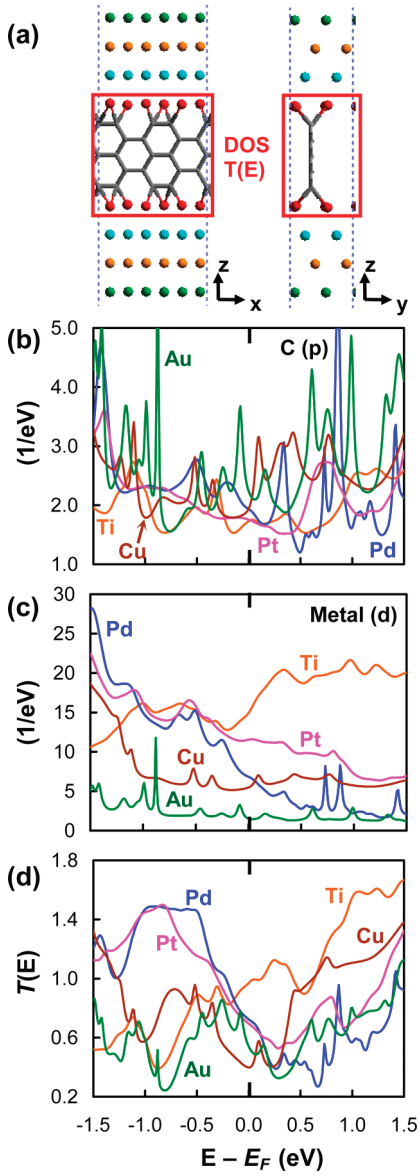

Figure 4. Current−voltage ($I-V$) calculations. (a) metal−graphene−metal structures used in $I-V$ calculations (Pd case shown). (b) Partial density of states (PDOS) for the p orbital for carbon at the metal−graphene interface per unit cell. (c) PDOS summing over all five d orbitals for metal at the metal−graphene interface per unit cell. (d) Transmission coefficient ($T(E)$) (orange, Ti; blue, Pd; pink, Pt; brown, Cu; green, Au). Separate lines of each metal for parts b, c, and d are shown in the Supporting Information (Figures S2, S3, and S4). E_F is the Fermi energy of the electrode.

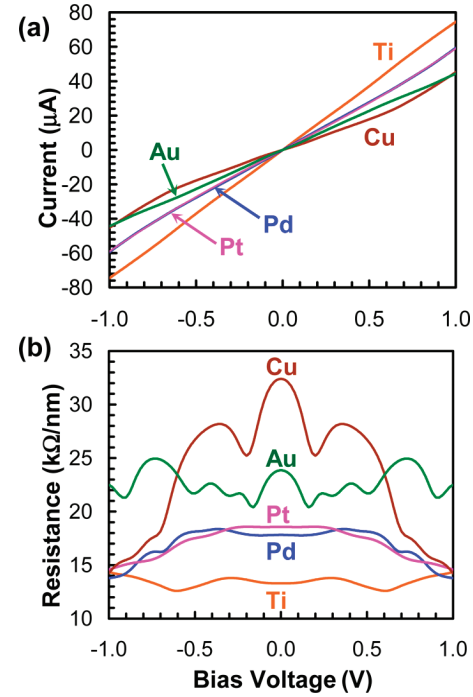

Figure 5. Current−voltage ($I-V$) characteristics near the Fermi energy per unit cell: (a) $I-V$ curve; (b) contact resistance (orange, Ti; blue, Pd; pink, Pt; brown, Cu; green, Au).

TABLE 2: Comparison of the Calculated Contact Resistances of "End-Contacted" and "Side-Contacted" Metal−Graphene Interfaces[a]

	Ti	Pd	Pt	Cu	Au
"end-contacted" per unit cell (kΩ)	13.3	17.8	18.6	31.7	23.3
"end-contacted" per C atom[b] (kΩ)	106.5	142.4	148.5	253.5	186.8
"side-contacted" per C atom[c] (kΩ)	938	8566	34 689	630 352	1 261 002

[a] For comparison, the contact resistance is averaged over the C atoms (eight atoms) at the interface. [b] Per surface C atom (16 atoms) at the interface. [c] Per surface C atom.[24]

We find that Ti has a linear $I-V$ curve from −1 to +1 V, indicating an Ohmic contact, while Pd and Pt are linear from −0.5 to +0.5 V.

Using the slope at the Fermi energy (0 V), we calculate conductance, leading to values ranging from 0.97 G_0 for Ti down to 0.40 G_0 for Cu. The conductance quantum for a single-walled carbon nanotube (SWNT) is expected to be 2 G_0 ($G_0 \equiv 2q^2/h = 77.5\ \mu S = (12.9\ k\Omega)^{-1}$), assuming perfect contacts. Thus, these end-contacted systems lead to 20−50% of the maximum conductance.

From the conductance we calculate the contact resistance (R_{cont}) per unit cell of the "end-contact" structures to be 53 kΩ for Ti, 71 kΩ for Pd, 74 kΩ for Pt, 127 kΩ for Cu, and 93 kΩ for Au after averaging the bias voltage from −0.1 to +0.1 V (Table 2). These contact resistances are also normalized per surface C atom at the interface to enable estimates for the contact resistance of "end-contacted" metal−CNT interfaces, as discussed below. As expected, the R_{cont} value of "end-contacted" is enormously improved over that of "side-contacted" electrodes with improvements ranging from best for Au (1/6751) followed by Cu (1/2488) > Pt (1/233) > Pd (1/60) > Ti (1/8.8).

4. Discussion

4.1. Nature of the Metal−Carbon Contact. With "side-contacted" metal−graphene interfaces, only the carbon p□ orbitals of carbon atoms contribute to the cohesion to the surface metals (d orbitals). However, for "end-contacted" metal−graphene interfaces, carbon pπ orbitals as well as pσ orbitals play important roles in cohesion because the surface carbon has pσ electrons that are either unpaired (zigzag) or involved in a weakened in-plane π bond (armchair). Thus, these pσ electrons are expected to play substantial roles in cohesion and hence transmission. In fact, Figure S1 of the Supporting Information shows that only the pπ orbital is important for transmission in Ti, Pd, and Pt while both the pπ and pσ orbitals are significant for transmission in Au and Cu electrodes. Additionally, the PDOS(C_p) of Au is smaller than the PDOS(M_d) near the Fermi energy.

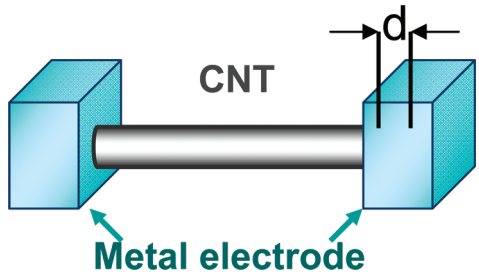

Figure 6. Proposed metal−CNT configuration.

4.2. Electrical Properties at the Interface. Our results indicate that, among the five metals considered here, the contact resistance per surface C atom is smallest for Ti (106 kΩ), small for Pd (142 kΩ) and Pt (149 kΩ), and large for Au (187 kΩ) and Cu (253 kΩ).

Recently, four-terminal experiments were reported for Pt electrodes (5 nm thickness and 200 nm width deposited on top of the CNT and protected with 60 nm Au) "side-contacted" to metallic SWNT (1.0−1.5 nm). They found a contact resistance of $R_{\text{side-cont}} \approx 5$ kΩ with a CNT length between contacts of ∼1 μm.[33] Assuming their CNT to be SWNT (10,10) (diameter = 1.37 nm) with the electrode contacts about half of the CNT circumference, the carbon atoms in with electrodes, this 200 nm electrode would be in contact with $N_{\text{side-cont}} = 8{,}096$ carbon atoms. Thus, we estimate the contact resistance per carbon atom, $Rc_{\text{side-cont}} = R_{\text{side-cont}} \times N_{\text{side-cont}} = 5000 \times 8096 = 40.5$ MΩ. This can be compared with our previous calculations for Pt side-contacted to graphene which led to $Rc_{\text{side-cont}} = 35.7$ MΩ per carbon atom (Table 2).[24] There is excellent agreement between experimental results and calculation results.

The contact resistance results calculated for the "end-contacted" metal−graphene interface can be used straightforwardly to estimate the contact resistance for the "end-contacted" metal−CNT interface. For example, the armchair SWNT (10,10) has 40 carbon atoms at the metal−CNT interfaces. Thus, since the calculated contact resistance per carbon atom for Pt−graphene results is $Rc_{\text{end-cont}} = 148.5$ kΩ, we estimate that the contact resistance of the "end-contacted" Pt−(10,10) SWNT interface would be $R_{\text{end-cont}} = 148.5/40 = 3.7$ kΩ, indicating that "end-contacted" Pt electrodes (with infinitesimal contact lengths) have the same contact resistance as 5 nm of "side-contacted" Pt electrode (∼5 kΩ).

Consider now a double-walled carbon nanotube (DWNT), for example, (10,10) and (6,6). Here, the number of the carbon atoms "end-contacted" with electrodes is 64, leading to $R_{\text{end-cont}} = 2.3$ kΩ. Thus the "end-contacted" electrodes are utilized quite effectively for multiwalled CNTs and CNT bundles.

Despite the advantages of "end-contacted" configurations, significant experimental difficulties remain in constructing them. Experiments to suspend and disperse CNTs in various solutions (e.g., water or organic solvents)[34−36] have been reported. For via (vertical) interconnects, chemical mechanical polishing has been successful in achieving "end-contacted" electrodes.[29] Combining such techniques may lead to development of similar approaches for horizontal "end-contacted" configurations.

As an alternative strategy, we consider the geometry where the electrode is deposited such that the end and part of the side of the CNT (Figure 6). In this case, the total contact resistance can be written as $R_{\text{cont}} = (1/R_{\text{end-cont}} + 1/R_{\text{side-cont}})^{-1}$, where $R_{\text{end-cont}} = Rc_{\text{end-cont}}/N_{\text{end-cont}}$ is from the "end-contacted" interfaces and $R_{\text{side-cont}} = Rc_{\text{side-cont}}/N_{\text{side-cont}}$ is from the "side-contacted" interfaces. Thus, for the case of a (10,10) SWNT, $N_{\text{end-cont}} = 40$, while $N_{\text{side-cont}} = 162$ for 10 nm. Since $Rc_{\text{end-cont}} = 142.4$ kΩ and $Rc_{\text{side-cont}} = 8566$ kΩ for Pd electrodes, we obtain a total contact resistance of $R_{\text{cont}} = 3.3$ kΩ. This illustrates the advantage of such "end-contacted" configurations. We assumed here a "side-contacted" length of 10 nm, since by the time it is necessary to use CNTs for via and horizontal interconnect components we expect that it will be necessary to reduce the contact area to 20 nm or less.

5. Conclusion

The small size and variations in device geometries have made it very difficult to extract reproducible results for the contact resistance of metal−CNT or metal−graphene interfaces. This makes it most valuable to develop and validate first-principles QM calculations to predict such quantities, since QM would provide consistent accuracy for various combinations of metals and carbon structures. This paper illustrates how to use first-principles QM to predict such complex phenomena as contact resistance in metal−graphene and metal−CNT assemblies, enabling in silico analysis and design prior to experiments.

On the basis of these QM studies of the graphene−metal interface, we conclude that there are substantial advantages in reduced contact resistances for configurations that include "end-contacted" metal electrodes. Because of the difficulty in making end-contacted electrodes as in Figure 1a, we suggest Figure 6 as practical configurations which also dramatically reduce the total contact resistance.

Although the application here is toward high-performance on-chip interconnect applications, the results should be applicable to other CNT or graphene based nanoelectronic and optoelectronic devices such as the field-effect transistors and light emitting diodes.

Acknowledgment. This work was supported partially by Intel Components Research (Kevin O'Brien, Florian Gstrein, and James Blackwell) and by the National Science Foundation (CCF-0524490 and CTS-0608889). The computer systems used in this research were provided by ARO-DURIP and ONR-DURIP. Additional support for the MSC was provided by ONR, ARO, DOE, NIH, Chevron, Boehringer-Ingelheim, Pfizer, Allozyne, Nissan, Dow-Corning, and DuPont, with additional support by the Functional Engineered Nano Architectonics (FENA) via the Microelectronics Advanced Research Corporation (MARCO) with the prime award (2009-NT-2048) at UCLA (PI Kang Wang).

Supporting Information Available: The detailed orbital contributions of the partial density of states (PDOS) of d orbitals of the surface metal atoms and p orbitals of the surface carbon atoms at the contact interface are shown in Figure S1 for each metal separately.

Also, the PDOS (Figure 3b and c) and the transmission coefficient, $T(E)$ (Figure 3d), are shown for each metal independently in Figures S2, S3, and S4, respectively. This material is available free of charge via the Internet at http://pubs.acs.org.

References and Notes

(1) Saito, R.; Dresselhaus, G.; Dresselhaus, M. S. *Physical Properties of Carbon Nanotubes*; Imperial College Press: London, 1998.

(2) Novoselov, K. S.; Geim, A. K.; Morozov, S. V.; Jiang, D.; Zhang, Y.; Dubonos, S. V.; Grigorieva, I. V.; Firsov, A. A. *Science* **2004**, *306*, 666.

(3) Novoselov, K. S.; Geim, A. K.; Morozov, S. V.; Jiang, D.; Katsnelson, M. I.; Grigorieva, I. V.; Dubonos, S. V.; Firsov, A. *Nature* **2005**, *438*, 197.

(4) Ohta, T.; Bostwick, A.; Seyller, T.; Horn, K.; Rotenberg, E. *Science* **2006**, *313*, 951.

(5) Oostinga, J. B.; Heersche, H. B.; Liu, X.; Morpurgo, A. F.; Vandersypen, L. M. K. *Nat. Mater.* **2008**, *7*, 151.

(6) Berger, C.; Song, Z.; Li, X.; Wu, X.; Brown, N.; Naud, C.; Mayou, D.; Li, T.; Hass, J.; Marchenkov, A. N.; Conrad, E. H.; First, P. N.; de Heer, W. A. *Science* **2006**, *312*, 1191.

(7) Chen, Z.; Lin, Y.-M.; Rooks, M. J.; Avouris, P. *Physica E* **2007**, *40*, 228.

(8) Naeemi, A.; Sarvati, R.; Meindl, J. D. *IEDM Dig.* **2004**, 699–702.

(9) Avouris, P. *Acc. Chem. Res.* **2002**, *35*, 1026.

(10) Avouris, P.; Chen, J. *Mater. Today* **2006**, *9*, 46.

(11) Yao, Z.; Kane, C. L.; Dekker, C. *Phys. Rev. Lett.* **2000**, *84*, 2941.

(12) Javey, A.; Guo, J.; Wang, Q.; Lundstrom, M.; Dai, H. *Nature* **2003**, *424*, 654.

(13) Mann, D.; Javey, A.; Kong, J.; Wang, Q.; Dai, H. *Nano Lett.* **2003**, *3*, 1541.

(14) Frank, S.; Poncharal, P.; Wang, Z. L.; de Heer, W. A. *Science* **1998**, *280*, 1744.

(15) Hone, J.; Yenilemez, E.; Tinbker, T. W.; Kim, W.; Dai, H. *Phys. Rev. Lett.* **2001**, *87*, 106801.

(16) Awano, Y.; Sato, S.; Kondo, D.; Ohfuti, M.; Kawabata, A.; Nihei, M.; Yokoyama, N. *Phys. Status Solidi A* **2006**, *203*, 3611.

(17) Xu, T.; Wang, Z.; Miao, J.; Chen, X.; Tan, C. M. *Appl. Phys. Lett.* **2007**, *91*, 042108.

(18) Coiffic, J. C.; Fayolle, M.; Maitrejean, S.; Foa Torres, L. E. F.; Le Poche, H. *Appl. Phys. Lett.* **2007**, *91*, 252107.

(19) Close, G. F.; Yasuda, S.; Paul, B.; Fujita, S.; Phillip Wong, H.-S. *Nano Lett.* **2008**, *8*, 706.

(20) Balandin, A. A.; Ghosh, S.; Bao, W.; Calizo, I.; Teweldebrhan, D.; Miao, F.; Lau, C. N. *Nano Lett.* **2008**, *8*, 902.

(21) Ghosh, S.; Calizo, I.; Teweldebrhan, D.; Pokatilov, E. P.; Nika, D. L.; Balandin, A. A.; Bao, W.; Miao, F.; Lau, C. N. *Appl. Phys. Lett.* **2008**, *92*, 151911.

(22) Brar, V. W.; Zhang, Y.; Yayon, Y.; Ohta, T.; McChesney, J. L.; Bostwick, A.; Rotenberg, E.; Horn, K.; Crommie, M. F. *Appl. Phys. Lett.* **2007**, *91*, 122102.

(23) Vazquez de Parga, A. L.; Calleja, F.; Borca, B.; Passeggi, M. C. G., Jr.; Hinarejos, J. J.; Guinea, F.; Miranda, R. *Phys. Rev. Lett.* **2008**, *100*, 056807.

(24) Matsuda, Y.; Wei-Qiao, D.; Goddard, W. A., III. *J. Phys. Chem. C* **2007**, *111*, 11113.

(25) Matsuda, Y.; Wei-Qiao, D.; Goddard, W. A. *J. Phys. Chem. C* **2008**, *112*, 11042.

(26) McEuen, P. L.; Fuhrer, M. S.; Park, H. *IEEE Trans. Nanotechnol.* **2002**, *1*, 78.

(27) Schultz, P. A. *Phys. Rev. Lett.* **2000**, *84*, 1942–1945. See also http://dft.sandia.gov/Quest/.

(28) Mattsson, A. E.; Schultz, P. A.; Desjarlais, M. P.; Mattsson, T. R.; Leung, K. *Modell. Simul. Mater. Sci. Eng.* **2005**, *13*, R1–R31.

(29) Perdew, J. P.; Burke, K.; Ernzerhof, M. *Phys. Rev. Lett.* **1996**, *77*, 3865.

(30) Kim, Y. -H.; Tahir-Kheli, J.; Schultz, P. A.; Goddard, W. A., III. *Phys. Rev. B* **2006**, *73*, 235419.

(31) Deng, W.-Q.; Muller, R. P.; Goddard, W. A., III. *J. Am. Chem. Soc.* **2004**, *126*, 13562–13563.

(32) *CRC Handbook of Chemistry and Physics*, 87th ed.; Lide, D. R., Ed.; CRC Press: Boca Raton, FL, 2006.

(33) Kanbara, T.; Takenobu, T.; Takahashi, T.; Iwasa, Y.; Tsukagori, K.; Aoyagi, Y.; Kataura, H. *Appl. Phys. Lett.* **2006**, *88*, 053118.

(34) Chen, J.; Hamon, M. A.; Hu, H.; Chen, Y.; Rao, A. M.; Eklund, P. C.; Haddon, R. C. *Science* **1998**, *282*, 95.

(35) Niyogi, S.; Hu, H.; Hamon, M. A.; Bhowmik, P.; Zhao, B.; Rozenzhak, S. M.; Chen, J.; Itkis, M. E.; Meier, M. S.; Haddon, R. C. *J. Am. Chem. Soc.* **2001**, *123*, 733. Zhao, B.; Hu, H.; Niyogi, S.; Itkis, M. E.; Hamon, M. A.; Bhowmik, P.; Meier, M. S.; Haddon, R. C. *J. Am. Chem. Soc.* **2001**, *123*, 11673.

(36) Strano, M. S.; Dyke, C. A.; Usrey, M. L.; Barone, P. W.; Allen, M. J.; Shan, H.; Kittrell, C.; Hauge, R. H.; Tour, J. M.; Smalley, R. E. *Science* **2003**, *301*, 1519.

JP806437Y